

Time-resolved surface plasmon polariton coupled exciton and biexciton emission

Yikuan Wang, Tianyu Yang, Mahshid Pourmand, Jacob J. Miller, Mark T. Tuominen, and Marc Achermann*

Physics Department, University of Massachusetts Amherst, 666 N. Pleasant Street, Amherst, MA 01003, USA
*achermann@physics.umass.edu

Abstract: We discuss the coupling between optically excited semiconductor nanocrystals (NC) and thin metal films in both the single and multi-exciton regime. Using time-resolved photoluminescence spectroscopy, we determine the decay dynamics of free space and surface plasmon polariton (SPP) coupled emission. The two dynamics are found to be distinctly different at very small NC-metal separations and at photon energies close to the SPP resonance frequency. A comparison with numerical calculations allow us to conclude that the difference in emission dynamics is associated with the different interactions of parallel and perpendicular dipole emitters with lossy surface waves. Experiments at high excitation densities reveal that the coupling to SPPs and lossy surface waves is identical for excitons and biexcitons.

©2010 Optical Society of America

OCIS codes: (250.5403) Plasmonics; (300.6500) Spectroscopy, time-resolved.

References and links

1. J. N. Farahani, D. W. Pohl, H. J. Eisler, and B. Hecht, "Single quantum dot coupled to a scanning optical antenna: a tunable superemitter," *Phys. Rev. Lett.* **95**(1), 017402 (2005).
2. P. Anger, P. Bharadwaj, and L. Novotny, "Enhancement and quenching of single-molecule fluorescence," *Phys. Rev. Lett.* **96**(11), 113002 (2006).
3. K. R. Catchpole, and A. Polman, "Plasmonic solar cells," *Opt. Express* **16**(26), 21793–21800 (2008).
4. Y. Wang, T. Yang, M. T. Tuominen, and M. Achermann, "Radiative rate enhancements in ensembles of hybrid metal-semiconductor nanostructures," *Phys. Rev. Lett.* **102**(16), 163001 (2009).
5. M. A. Noginov, G. Zhu, A. M. Belgrave, R. Bakker, V. M. Shalae, E. E. Narimanov, S. Stout, E. Herz, T. Suteewong, and U. Wiesner, "Demonstration of a spaser-based nanolaser," *Nature* **460**(7259), 1110–1112 (2009).
6. R. F. Oulton, V. J. Sorger, T. Zentgraf, R. M. Ma, C. Gladden, L. Dai, G. Bartal, and X. Zhang, "Plasmon lasers at deep subwavelength scale," *Nature* **461**(7264), 629–632 (2009).
7. R. J. Walters, R. V. A. van Loon, I. Brunets, J. Schmitz, and A. Polman, "A silicon-based electrical source of surface plasmon polaritons," *Nat. Mater.* **9**(1), 21–25 (2010).
8. J. Bellessa, C. Bonnard, J. C. Plenet, and J. Mugnier, "Strong coupling between surface plasmons and excitons in an organic semiconductor," *Phys. Rev. Lett.* **93**(3), 036404 (2004).
9. Y. Fedutik, V. V. Temnov, O. Schöps, U. Woggon, and M. V. Artemyev, "Exciton-plasmon-photon conversion in plasmonic nanostructures," *Phys. Rev. Lett.* **99**(13), 136802 (2007).
10. A. V. Akimov, A. Mukherjee, C. L. Yu, D. E. Chang, A. S. Zibrov, P. R. Hemmer, H. Park, and M. D. Lukin, "Generation of single optical plasmons in metallic nanowires coupled to quantum dots," *Nature* **450**(7168), 402–406 (2007).
11. J. Grandidier, G. C. des Francs, S. Massenot, A. Bouhelier, L. Markey, J. C. Weeber, C. Finot, and A. Dereux, "Gain-assisted propagation in a plasmonic waveguide at telecom wavelength," *Nano Lett.* **9**(8), 2935–2939 (2009).
12. J. Homola, S. S. Yee, and G. Gauglitz, "Surface plasmon resonance sensors: review," *Sens. Actuators B Chem.* **54**(1-2), 3–15 (1999).
13. K. H. Drexhage, "Interaction of light with monomolecular dye layers," in *Progress in Optics*, E. Wolf, ed. (North-Holland, Amsterdam, 1974).
14. I. Gryczynski, J. Malicka, Z. Gryczynski, and J. R. Lakowicz, "Surface Plasmon-Coupled Emission with Gold Films," *J. Phys. Chem. B* **108**(33), 12568–12574 (2004).
15. I. Gryczynski, J. Malicka, W. Jiang, H. Fischer, W. C. W. Chan, Z. Gryczynski, W. Grudzinski, and J. R. Lakowicz, "Surface-plasmon-coupled emission of quantum dots," *J. Phys. Chem. B* **109**(3), 1088–1093 (2005).
16. A. Bouhelier, and G. P. Wiederrecht, "Excitation of broadband surface plasmon polaritons: Plasmonic continuum spectroscopy," *Phys. Rev. B* **71**(19), 195406 (2005).

17. H. Raether, *Surface plasmons on smooth and rough surfaces and on gratings* (Springer-Verlag, Berlin; New York, 1987).
18. M. Achermann, M. A. Petruska, S. A. Crooker, and V. I. Klimov, "Picosecond energy transfer in quantum dot Langmuir-Blodgett nanoassemblies," *J. Phys. Chem. B* **107**(50), 13782–13787 (2003).
19. G. W. Ford, and W. H. Weber, "Electromagnetic interactions of molecules with metal surfaces," *Phys. Rep.* **113**(4), 195–287 (1984).
20. R. R. Chance, A. Prock, and R. Silbey, "Lifetime of an Emitting Molecule near a Partially Reflecting Surface," *J. Chem. Phys.* **60**(7), 2744–2748 (1974).
21. I. A. Larkin, M. I. Stockman, M. Achermann, and V. I. Klimov, "Dipolar emitters at nanoscale proximity of metal surfaces: Giant enhancement of relaxation in microscopic theory," *Phys. Rev. B* **69**(12), 121403 (2004).
22. M. G. Bawendi, S. A. Empedocles, and R. Neuhauser, "Three-dimensional orientation measurements of symmetric single chromophores using polarization microscopy," *Nature* **399**(6732), 126–130 (1999).
23. A. V. Malko, A. A. Mikhailovsky, M. A. Petruska, J. A. Hollingsworth, H. Htoon, M. G. Bawendi, and V. I. Klimov, "From amplified spontaneous emission to microring lasing using nanocrystal quantum dot solids," *Appl. Phys. Lett.* **81**(7), 1303–1305 (2002).
24. S. E. Yalcin, Y. Wang, and M. Achermann, "Spectral bandwidth and phase effects of resonantly excited ultrafast surface plasmon pulses," *Appl. Phys. Lett.* **93**(10), 101103 (2008).
25. V. I. Klimov, "Optical nonlinearities and ultrafast carrier dynamics in semiconductor nanocrystals," *J. Phys. Chem. B* **104**(26), 6112–6123 (2000).
26. M. Achermann, J. A. Hollingsworth, and V. I. Klimov, "Multiexcitons confined within a subexcitonic volume: Spectroscopic and dynamical signatures of neutral and charged biexcitons in ultrasmall semiconductor nanocrystals," *Phys. Rev. B* **68**(24), 245302 (2003).
27. V. I. Klimov, A. A. Mikhailovsky, D. W. McBranch, C. A. Leatherdale, and M. G. Bawendi, "Quantization of multiparticle Auger rates in semiconductor quantum dots," *Science* **287**(5455), 1011–1013 (2000).
28. B. Yang, J. E. Schneeloch, Z. Pan, M. Furis, and M. Achermann, "Radiative lifetimes and orbital symmetry of electronic energy levels of CdS nanocrystals: Size dependence," *Phys. Rev. B* **81**(7), 073401 (2010).

1. Introduction

Coupling between dipole emitters and metal nanostructures at optical frequencies allows control over the flow of electromagnetic energy on the nano- and micrometer length scale [1–10]. For example, such coupling has been used to demonstrate enhanced emission and absorption of emitters [1–4], plasmon lasers [5,6], and the successful implementation of electrically pumped surface plasmon polariton (SPP) emitters [7]. The coupling is of particular interest since the hybrid materials combine components with complementary properties: high emission yields of many dipole emitters and strong electromagnetic field concentrations in metal nanostructures that act as intermediates between photons and the atomic and molecular length scale.

In this report we focus on the interactions between dipole emitters and plane metal films that are in close proximity. This basic configuration is important for studying the excitation and amplification of SPPs [6,11] and designing SPP-based sensors [12]. Several decades ago, first experiments showed that the fluorescence lifetime of a dipole emitter near a metal surface is greatly modified by the reflection and absorption of the metal surface [13]. At large separations between the emitter and the metal surface, the fluorescence lifetime oscillates as a function of separation, while at small separations the lifetime monotonically decreases when the dipole approaches the metal surface [13]. The oscillations are due to the metal surface acting as a mirror for the electric field of the emitter. The interference between the reflected wave and the initial wave gives rise to the observed oscillations in the lifetime. The lifetime decrease at small dipole-metal separations is due to non-radiative energy transfer from the excited dipole to the metal that leads to the excitation of SPPs and lossy surface waves. Both energy transfer mechanisms are of non-radiative nature; however, the energy transferred to the SPPs can be recovered in the appropriate geometry that allows momentum match with photons, resulting in surface plasmon coupled emission (SPCE) [8,14,15]. Although SPCE has been characterized previously, only few reports addressed the dynamic of the coupling between emitters and SPPs and how it compares with time-resolved free space emission (FSE) [9,10,14]. All these investigations were performed in the low excitation power or linear regime and in the discussion of the SPP dynamics the orientation of the dipole emitter with respect to the metal structure was not considered. Here, we discuss how excited semiconductor nanocrystals (NCs) with different sizes and emission wavelengths couple to proximal thin metal films in the low and high excitation regime. Comparing FSE and SPCE

dynamics allows us to distinguish the coupling of perpendicular and parallel emission dipoles near the metal surface as a function of photon energy. Moreover, using high-intensity excitation pulses we determine the biexciton-metal coupling and compare it with the coupling between single excitons and metal films.

2. Experimental setup

To study the interaction of excited NCs with thin metal films we purchased from NN-labs two types of CdSe/ZnS core/shell NCs with emission peaks centered at 560 and 630 nm [Fig. 1(a)]. The NCs were spin-coated as sub-monolayers onto thin metal films with or without an additional dielectric spacer layer. Gold films of 50 nm thickness on glass cover slips were purchased from Platypus Technologies, while silver films of similar thickness were produced on cover slips by electron beam evaporation. The same technique was used to add the silicon oxide spacer layer on top of the metal films. The thickness of the dielectric spacer layer and the coverage of NCs were determined by atomic force measurements. The functionalized glass slides were attached to a glass half sphere and optically matched with index matching fluid. Since the thickness of the glass cover slip (< 0.2 mm) is much smaller than the radius of the half sphere (5 mm), the half-spherical symmetry of the configuration is not significantly altered. The symmetry that comes with the use of a half sphere facilitates the analysis and alignment of the experiment. The NCs are excited in the center of the half sphere with short laser pulses and the emission is detected at different angles using the setup shown in Fig. 1(b). We use different lasers and excitation geometries for the single and multiexciton regimes, which will be explained in the respective sections below. The emission is collected with a lens and refocused onto an optical fiber on a rotation stage that allows us to measure FSE normal to the sample surface and SPPE at the well-defined SPP-coupling angle on the half sphere side of the sample [Fig. 1(b)]. We would like to emphasize that the emission on the half sphere side is highly p-polarized and is measureable only at a well defined angle from the sample normal that confirms the assignment of the detected signal to SPPE [8,14,15]. The sample and the excitation source are kept fixed for FSE and SPPE measurements. The numerical aperture of the lens results in an angular resolution of $\sim 8^\circ$. The optical fiber is coupled to a monochromator that spectrally resolves the emission. As a result of the inhomogeneous broadened NC emission, we are able to probe the spectral range from 530 to 660 nm with the two NC samples [Fig. 1(a)]. The decay dynamics of the emission is obtained with a time correlated single photon counting system (TCSPC) that provides sub-100 ps time resolution.

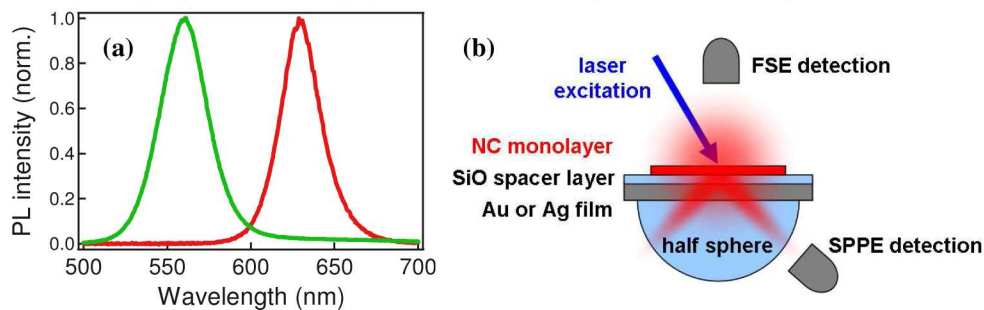


Fig. 1. (a) Photoluminescence (PL) spectra of two NC samples with center wavelengths of 560 and 630 nm. (b) Schematic of the setup, showing the two detector positions to measure SPPE and FSE dynamics.

3. Theoretical and numerical modeling of SPPE and FSE decay dynamics

Emitters in the close proximity of a metal surface can excite SPPs that can decay radiatively and lead to SPPE [14]. The generation of SPPE can be divided into two steps that are energy transfer (ET) from excited emitters to SPPs and the radiative decay of SPPs. ET between the

emitter and the SPP occurs when the emitter is within the evanescent field of the SPP that decays exponentially within typically 100 nm into the dielectric half space on the emitter-side of the metal surface. Upon excitation the SPPs decay both through non-radiative and radiative channels on a sub-ps time scale in the wavelength range considered here. The non-radiative decay is caused by intrinsic ohmic losses in the metal and surface roughness, while the radiative decay rate strongly depends on the sample geometry. In our sample configuration, SPPs are excited on the NC-side of the metal surface and decay into photons that propagate through the half sphere [8,15]. It can be calculated that the radiative decay of SPPs occurs with a rate that is 2-5 times smaller than the non-radiative decay rate in the wavelength range considered here [16]. The radiative decay path is enabled because of SPP-photon energy and momentum matching and results in p-polarized SPPE at a well defined angle θ_{SPP} near 45° [Eq. (1)]. This coupling angle is determined by the SPP dispersion relation and depends on the emission wavelength and the thickness of the dielectric spacer layer. For a simple case of a metal film with dielectric function ϵ_m that is facing air on one side and glass with refractive index n_{glass} on the other side, θ_{SPP} is given by [17]

$$n_{glass} \sin(\theta_{SPP}) = \sqrt{\frac{\epsilon_m}{1 + \epsilon_m}}. \quad (1)$$

The dynamics of SPPE can be determined by modeling the dynamics of the number of excited NCs and SPP modes, N_{NC} and N_{SPP} , with the following coupled rate equations:

$$\frac{dN_{NC}}{dt} = g(t) - (\Gamma_{ET} + \Gamma_{NC})N_{NC}(t), \quad \text{and} \quad \frac{dN_{SPP}}{dt} = \Gamma_{ET}N_{NC}(t) - \Gamma_{SPP}N_{SPP}(t), \quad (2)$$

in which $g(t)$ represents the exciton generation by the laser pulse, Γ_{ET} is the NC-SPP ET rate, Γ_{NC} is the decay rate of the NC excitation without NC-SPP ET effects, and Γ_{SPP} is the SPP decay rate. This model is conceptually similar to the description of a donor-acceptor system. The decay rate Γ_{NC} contains all decay processes of a NC in the proximity of a metal surface except for the coupling to SPPs. Γ_{NC} is the sum of the radiative rate, intrinsic non-radiative rates caused by non-ideal NC surface passivation and energy transfer between neighboring NCs [18], and a non-radiative rate that describes coupling to lossy surface waves. The latter are high k-vector waves at the dielectric-metal interface that are strongly damped because of ohmic losses in the metal [19]. The coupling to lossy surface waves is the primary effect that leads to what is commonly known as emission quenching.

The dynamics of SPPE is governed by $N_{SPP}(t)$ and it can be shown by solving Eqs. (2) that $N_{SPP}(t)$ decays with a rate $\Gamma = \Gamma_{ET} + \Gamma_{NC}$, if $\Gamma_{SPP} > \Gamma$. This condition is satisfied here, since $\Gamma_{SPP} > 1 \text{ ps}^{-1}$ considering SPP propagation distances of tens to hundreds of micrometers [17] and $\Gamma < 0.01 \text{ ps}^{-1}$, as we will show below. Since the emission from NCs coupled to SPPs decays with the same rate Γ , the SPPE dynamics is a good monitor of the NC-metal coupling process. This interaction between a dipole emitter and a metal surface depends on many factors such as photon energy and metal-dipole separation, but also on the orientation of the dipole emitter [19,20]. If we decompose the randomly oriented NCs into NCs with parallel and perpendicular emission dipoles with respect to the metal surface, we can write the SPPE dynamics in the following way:

$$SPPE(t) \propto \Gamma_{ET}^{\perp} e^{-\Gamma^{\perp} t} + \Gamma_{ET}^{\parallel} e^{-\Gamma^{\parallel} t}, \quad (3)$$

in which Γ^{\perp} and Γ^{\parallel} are the total decay rates of perpendicular and parallel dipoles, respectively. In contrast, FSE that we detected exactly normal to the film surface originates from NCs with parallel emission dipoles, since perpendicular dipoles don't emit into the direction normal to the surface. Therefore the FSE dynamics can be written as

$$FSE(t) \propto e^{-\Gamma^{\parallel} t}. \quad (4)$$

Hence, a difference in decay dynamics between SPPE and FSE must originate from different decay rates of parallel and perpendicular emission dipoles. Such a difference is expected because the emitter orientation affects the strength of most decay channels that contribute to the total decay rate of a dipole emitter in the proximity of a metal surface. In Fig. 2 we show calculated decay rates of parallel and perpendicular dipoles and the decomposition of the total rate into contributions from radiative decay, ET to SPPs, and ET to lossy waves [19,20]. We considered a dipole emitter at a distance $d = 10$ nm from a gold surface and distinguished three dielectric environments for the dipole that are (a) in a half space of air, (b) at a dielectric/air interface, and (c) embedded in a thin dielectric layer (see Fig. 2). The rates are normalized to the radiative decay rate in the absence of the metal interface.

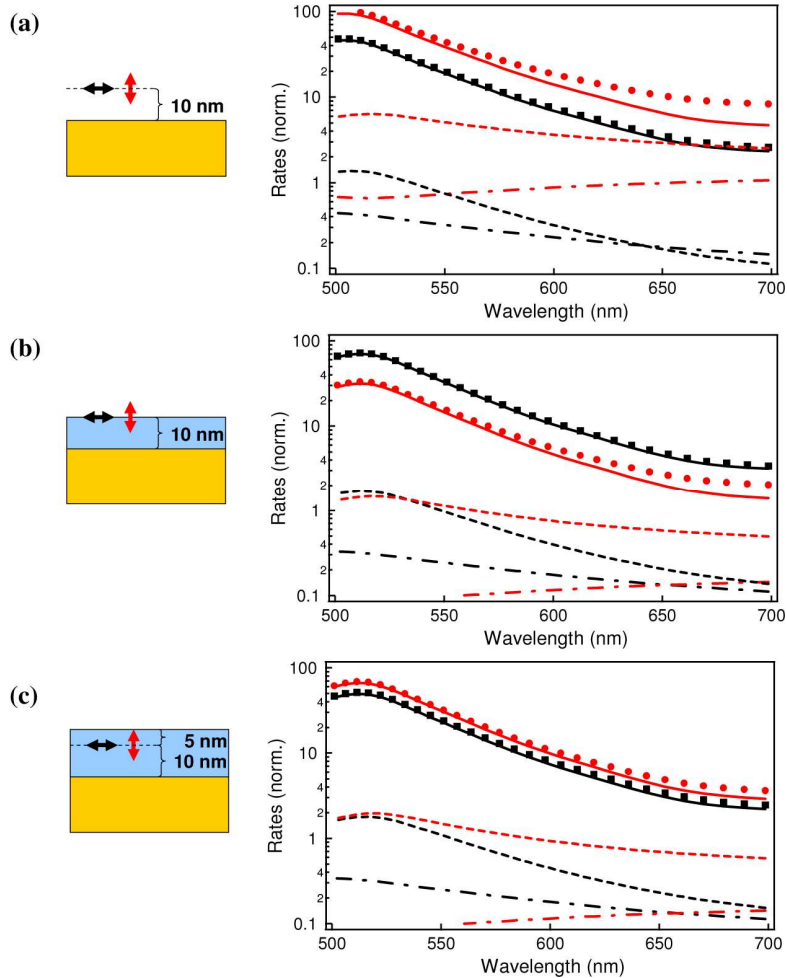


Fig. 2. Decay rates of parallel (black) and perpendicular (red) dipoles and the decomposition of the total rate (markers) into contributions from radiative decay (dash-dotted line), ET to SPPs (dashed line), and ET to lossy waves (solid line). The dipoles are located 10 nm from the gold surface and are either (a) in air, (b) at a dielectric/air interface, or (c) embedded in a thin dielectric layer. For the dielectric layer, we considered a refractive index of 1.46 (silicon oxide).

We notice that in all three cases shown in Fig. 2 the total decay rate is dominated by the ET rate to lossy surface waves, because of the short metal-dipole separation of 10 nm. Another common feature is that both ET rates to SPPs and lossy surface waves are enhanced at shorter wavelengths and peak at the SPP resonance wavelength around 510 nm. Most

interestingly, the relative contributions of perpendicular and parallel dipoles depend on the details of the dielectric environment of the dipole emitter in the close proximity of the metal surface. Specifically, in situations (a) and (c) perpendicular dipoles decay faster than parallel dipoles. In contrast, in situation (b) the decay rate of parallel dipoles is larger than the one of perpendicular dipoles. This switch in hierarchy is primarily caused by the dipole's interaction with lossy surface waves. In the following, we will use the presented theoretical discussion to describe our experimental results. While situation (a) was calculated to demonstrate the soundness of the calculations, situations (b) and (c) can be used to approximate our sample configuration.

4. SPPE and FSE dynamics in the single exciton regime

In the single exciton regime that is first discussed here, we excite the NCs with a low power diode laser that emits laser pulses at 407 nm with a repetition rate of 10 MHz. The pulse duration of ~60 ps and the response time of the TCSPC electronics lead to an instrument response time of ~80 ps. The excitation occurs from the front side of the sample at 30° off the surface normal in order to enable FSE detection normal to the surface [Fig. 1(b)]. At the excitation wavelength, all NCs in the monolayer can be excited independently of their crystalline orientation with respect to the excitation pulse direction and polarization, because the absorption of high-energy photons is caused by a dense manifold of electronic levels.

In Fig. 3 we compare time-resolved FSE and SPPE at 560 nm of NCs that were spin coated onto gold films with spacer layers of 5 and 12 nm, resulting in separations between the metal surface and the NC centers of $d \sim 10$ and 17 nm (considering the ligand length, the ZnS shell thickness and the CdS core radius). We notice that at short separations SPPE decays faster than FSE, while at larger NC-metal separations SPPE and FSE display the same decay dynamics.

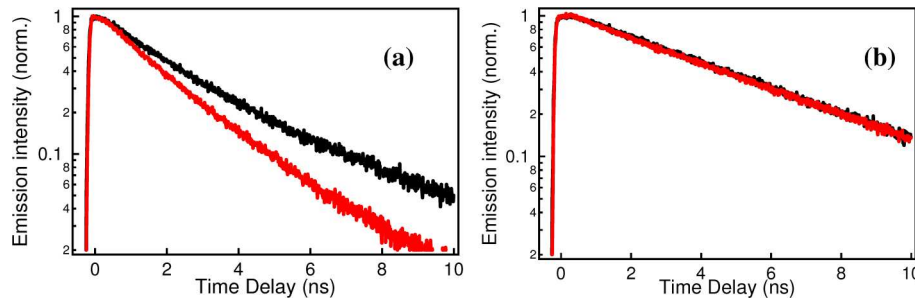


Fig. 3. FSE (black) and SPPE (red) decay dynamics recorded at 560 nm with different spacer layers that result in gold-dipole separations of ~10 nm (a) and ~17 nm (b).

Following the discussion in the previous section, we can assign the difference in SPPE and FSE decay dynamics to the difference in interaction strengths between parallel and perpendicular dipoles with the metal surface. For a quantitative discussion of this difference, we consider Eqs. (3) and (4) and obtain for the ratio between SPPE and FSE dynamics:

$$\frac{SPPE(t)}{FSE(t)} \propto e^{-\Delta\Gamma t} + constant, \quad (5)$$

in which $\Delta\Gamma = \Gamma^\perp - \Gamma^\parallel$. The advantage of this analysis is that it holds for ensembles of NCs with non-radiative decay channels, such as energy transfer between NCs [18]. Considering Eq. (5) we directly obtain the rate difference between perpendicular and parallel dipoles from the experimentally determined SPPE/FSE ratio by fitting the emission ratio with a single exponential function [Fig. 4(a)]. Figures 3 and 4 indicate that $\Gamma^\perp > \Gamma^\parallel$ at $d = 10$ nm, while there is no measurable decay rate difference between parallel and perpendicular emission dipoles at $d \sim 17$ nm.

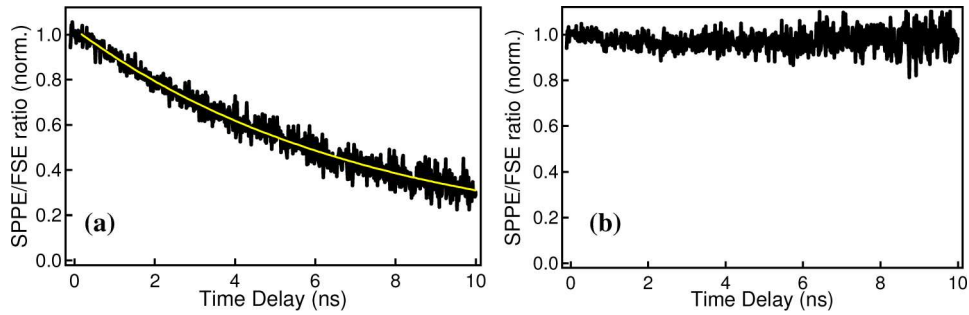


Fig. 4. SPPE/FSE ratio at 560 nm and $d \sim 10$ nm (a) and $d \sim 17$ nm (b). The yellow line in (a) is the best fit with a single exponential function.

Following the same procedure, we analyzed spectrally resolved FSE and SPPE dynamics of NC samples with emission peaks centered at 560 or 630 nm that were either deposited directly on the gold surface ($d \sim 5$ nm) or with a 5 or 12 nm spacer layer ($d \sim 10$ or 17 nm). In Fig. 5(a) we show the resulting decay rate differences. As indicated by Fig. 4(b), there was no measurable decay rate difference at $d \sim 17$ nm. At $d \sim 5$ and 10 nm, the decay rate difference is positive, meaning that perpendicular dipoles decay faster than parallel dipoles. Considering the numerical calculations in Fig. 2, our results indicate that modeling the NCs as point dipoles at a dielectric/air interface fails. A better correspondence between experimental and calculated results is obtained by considering that the emission dipoles are embedded in a dielectric layer [Fig. 2(c)]. In Fig. 5(b) we show calculated decay rate differences obtained from this model. The chosen thickness of 5 nm of the dielectric layer on top of the point dipoles corresponds to the total radius of the NCs including organic ligands. We find good agreement between experimental and theoretical results, which let us conclude that the model is appropriate for describing our experimental configuration.

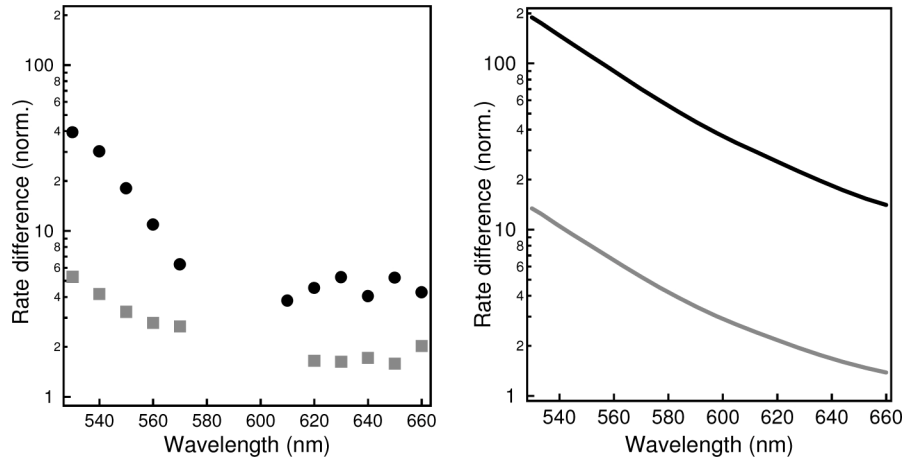


Fig. 5. (a) Spectrally resolved decay rate differences obtained from FSE and SPPE decay dynamics. The separations between the NC centers and the metal surface were approximately 5 nm (black circles) and 10 nm (grey squares). (b) Calculated decay rate difference between perpendicular and parallel dipoles for the same metal-dipole separations of 5 nm (black line) and 10 nm (grey line). The dielectric configuration shown in Fig. 2(c) was used.

Figure 5 shows that both experimental and theoretical decay rate differences increase at shorter wavelengths and peak at the SPP resonance wavelength. Our theoretical calculations in Fig. 2 indicate that the decay rate difference is primarily due to the coupling to lossy surface waves that is different for perpendicular and parallel dipoles. Although the radiative rate and the coupling to SPPs also depend on the dipole orientation, they contribute significantly less to the total decay rate difference in the wavelength and separation range of

our experiments. It is noteworthy that coupling to lossy surface waves as well as SPPs max out at the same frequency, since both effects are determined by the dielectric environment. The strong dependence on the dipole-metal separation supports the assignment of the decay rate difference to interactions with lossy surface waves. It has been shown that this interaction can be described by a d^{-3} or d^{-4} distance dependence [21]. The coupling to SPPs is less sensitive to small separation changes since the SPP field decays exponentially on a typical length scale of ~ 100 nm.

While theory and experiment agree well in magnitude and overall trend, differences between the measured and calculated decay rate can be assigned to the simplifications of the model that disregards any microscopic structure of the NCs and the degeneracy of the NC emission dipole [22] and assumes continuous and smooth layers with perfectly plane interfaces.

5. Surface plasmon polariton coupled emission in the multi-exciton regime

In the previous section we studied the interaction of single excitons with a proximal metal film that is of importance for sensor applications that make use of SPPE. In this section, we want to understand the interaction of biexcitons and a planar metal surface. NCs in the biexciton regime provide a high optical gain material [23] that can be used for amplifying SPPs [11]. To study such biexciton-metal interactions we employed the same setup and sample configuration as described above, but used a silver instead of a gold film and a laser source with sufficient power to generate biexcitons in the CdSe NCs that were deposited on the silver film. The excitation source was a frequency-doubled Ti-sapphire oscillator that operates at a repetition rate of 90 MHz and provides sub-50 fs pulses at 420 nm with pulse energies of ~ 0.2 nJ. Although corresponding pulse intensities are too low to excite multiexcitons in NCs directly, we achieve sufficiently high intensities by coupling the ultrafast laser pulses to SPPs using prism coupling [24]. We focused the excitation beam through the glass half sphere onto the silver film at the SPP-coupling angle, which enhances the electric field on the metal surface. For a 50 nm thick silver film with a 5 nm dielectric spacer layer we calculated a field enhancement factor of 5.7 at the dielectric/air interface yielding an intensity enhancement of 32. With such an enhancement we estimate that the excitation intensity is sufficient to excite biexcitons in large NCs that we used for these experiments. Based on the 1s absorption peak around 633 nm we estimate a NC radius of ~ 3.5 nm and a corresponding absorption cross section of 7×10^{-15} cm² at the excitation wavelength [25]. The field enhancement is the main motivation to conduct the high-intensity experiments with *silver* films, since the field is strongly attenuated in *gold* films at the excitation wavelength of ~ 420 nm.

The excitation of biexcitons in NCs can easily be detected by time-resolved spectroscopy. As a result of Coulomb interaction, the biexciton emission in CdSe NCs is red-shifted with regard to the exciton emission [26]. However, this shift is in general much smaller than the inhomogeneous broadening and, therefore, does not serve well as an indicator to distinguish biexciton from single exciton emission. In contrast, multiexciton interactions lead to short biexciton lifetimes in the range of tens to hundreds of ps due to non-radiative Auger recombination [27]. In this process one of the two excitons recombines by exciting the second exciton to a higher energy level. For a comparison, single excitons have a radiative lifetime in the order of 20 ns and, therefore, time-resolved spectroscopy lends itself well to distinguish biexciton from exciton emission.

In Fig. 6(a) we show SPPE obtained with different excitation intensities (the highest is 9 times stronger than the lowest intensity). Clearly visible is an acceleration of the SPPE with increasing excitation intensities at early time delays. Such acceleration of decay dynamics only occurs at high excitation levels and it is a clear indication of SPP coupled *biexciton* emission. At longer time delays the decay approaches the excitonic SPPE decay that is measured with low excitation intensities. To determine the interaction strength of biexcitons with the silver film, we followed the procedure described above and compared SPPE measured on the half sphere side of the sample with FSE detected normal to the surface. In

Fig. 6(b) we show the ratio SPPE/FSE that indicates the difference between the two dynamics. Interestingly, the dynamics of SPPE/FSE is independent of the excitation intensity, implying that the interaction of excitons and biexcitons with the metal surface is identical at the measured emission frequency. It has to be noted here that interactions between excitons/biexcitons and the silver film are not maximized, because the emission frequency is significantly smaller than the SPP resonance frequency of the silver film. Spectral overlap and, therefore, stronger interactions are expected with CdS NCs that emit in the blue and UV wavelength range [28].

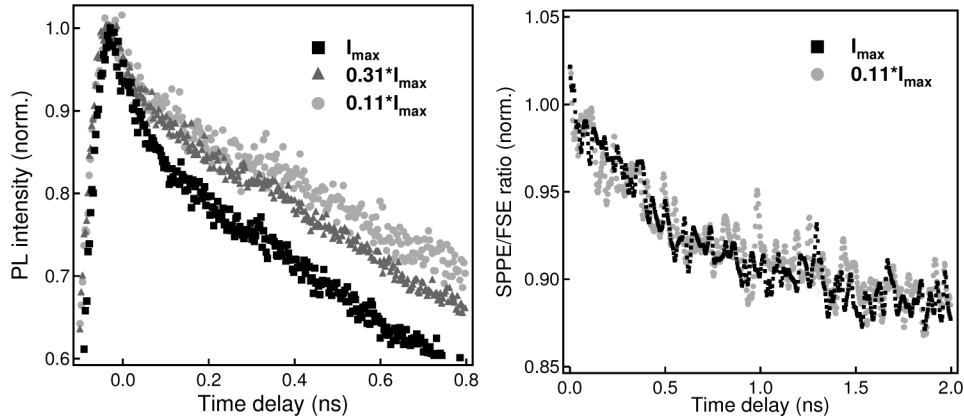


Fig. 6. (a) SPPE dynamics of NCs on a silver film that are excited with varying excitation intensities (emission wavelength is 646 nm). (b) SPPE/FSE ratio at low (grey circles) and high excitation densities (black squares) indicating identical coupling strength of biexcitons and excitons with the silver film.

6. Conclusion

In this work we have studied the interaction of dipole emitters with thin metal films by comparing the decay dynamics of free space and SPP coupled emission. We found that there is a distinct difference in emission dynamics that becomes more pronounced when the dipole emitters are within a few nanometers from the metal surface and when the emission frequency is close to the SPP resonance frequency. Comparing measurements with numerical calculations we concluded that the different dynamics can be assigned to a difference in coupling strength of parallel and perpendicular emission dipoles with lossy surface waves. The same experiments performed at high excitation levels revealed that the interactions of biexcitons and excitons with the metal surface are similar at frequencies that are off resonance with the SPP resonance frequency. The obtained insights into the interactions of emission dipoles with metal surfaces are of fundamental importance for NC-based SPP amplifiers and SPP-based sensors, specifically when used for single molecule detection with well defined dipole orientations.

Acknowledgments

This work was supported by the Defense Advanced Research Projects Agency (DARPA) and the National Science Foundation under the grant ECCS-0725609.